33RD INTERNATIONAL COSMIC RAY CONFERENCE, RIO DE JANEIRO 2013
THE ASTROPARTICLE PHYSICS CONFERENCE

ICRC 2013

Measurement of the muon signal using the temporal and spectral structure of the signals in surface detectors of the Pierre Auger Observatory

BALÁZS KÉGL[1], FOR THE PIERRE AUGER COLLABORATION[2]

[1] *Laboratoire de l'Accélérateur Linéaire, Université Paris Sud, CNRS/IN2P3, Orsay, France*
[2] *Full author list: http://www.auger.org/archive/authors_2013_05.html*
auger_spokespersons@fnal.gov

Abstract: Applying different filtering techniques to the temporal distribution of the signals measured with the Auger surface detector array (SD), we separate the electromagnetic and muonic signal components of air-showers. The filters are based on the different characteristics of the muonic and electromagnetic components in individual detectors, the former being composed of peaks above a smooth background due to the lower energy deposition of the latter photons and electrons. The muon signal is derived for showers of 10 EeV primary energy at a core distance of 1 km, with the aim of testing the predictions of hadronic interaction models. We compare the fraction of the muonic signal and the total signal to model predictions for proton and iron primaries in a range of zenith angles from 0 to 60°.

Keywords: Pierre Auger Observatory, ultra-high energy cosmic rays, muons, hadronic interactions

1 Introduction

Understanding the development of extensive air-showers in the atmosphere is of central importance for deriving information on cosmic rays such as their energy distribution and mass composition. At the same time, detailed measurements of the characteristics of air-showers allow us to probe particle interactions up to the highest energies. While electromagnetic interactions in air-showers are well understood, there are considerable uncertainties in simulating the production of hadronic particles at energies and for phase space regions not accessible in accelerator experiments [1]. This makes the study of the hadronic component of showers particularly important.

Both the electromagnetic and the muonic shower components are fed mainly by pions and kaons produced in the hadronic core of the showers. Photons produced in the decay of neutral pions give rise to electromagnetic subshowers in which further particle multiplication and interactions make the distributions of the initial energy and the production depth inaccessible to ground-based detectors. In contrast, muons suffer only a small energy loss and angular deflection before reaching ground, and so they provide a window to study the hadronic shower core.

In this work we we will use the water Cherenkov detectors of the SD of the Pierre Auger Observatory [2] to measure the number of muons arriving at ground in showers of $E = 10^{19}$ eV at a distance of 1000 m from the shower core. We will compare the data with predictions derived from showers simulated with the interaction models QGSJETII.04 [3] and EPOS LHC [4].

The measurement is based on the time profile and on spectral characteristics of the Cherenkov light signal generated by shower particles in the water of the detectors. We provide updates of methods presented previously [5, 6]. Improved understanding of the essential aspects of these methods and the homogeneity of the time signals in the small energy and distance intervals considered here made it possible to simplify the methods and to better control the systematics due to model uncertainties and the unknown chemical composition of the cosmic rays.

In Section 2 we describe the methods of deriving the signal fraction due to muons and, after discussing the data selection and corresponding Monte Carlo simulations in Section 3, we present the muon measurements in Section 4. The derived muon fraction is then used to obtain the signal of the muonic shower component. A summary is given in Section 5.

2 Methods of measuring the muon fraction

The Cherenkov photons produced by the shower particles in the detectors are sampled by three photomultipliers (PMTs) [2]. The analog signal is then digitized with FADCs in 25 ns bins with a 10 bit dynamic range. The raw digital signal of each PMT is calibrated such that the integrated signal of a typical vertical atmospheric muon is 1. The signal in each time bin is thus measured in units of "vertical equivalent muon" or VEM [7]. Finally, the three calibrated traces of the PMTs of each detector are averaged. We will denote the resulting FADC signal by $\mathbf{x} = (x_1, \ldots, x_N)$, where N is the number of time bins, and the total signal by $S = \sum_{j=1}^{N} x_j$. The total muonic and electromagnetic signals will be denoted by S_μ and $S_{\rm EM}$, respectively. Note that S_μ is the pure muonic signal, so the electromagnetic halo produced by muon interactions and muon decay in the atmosphere goes into $S_{\rm EM}$.

In the following we will derive the fraction f_μ of the signal that can be attributed to muons relative to the total signal S

$$f_\mu = S_\mu / S \qquad (1)$$

by exploiting the information on the temporal structure of the FADC signal at 1000 m from the shower core. Due to the similar energy scaling of the overall and muonic shower signals in the detectors at about 1000 m, this quantity is insensitive to the systematic uncertainty of the energy assigned to air-showers that is of the order of ∼14% [8].

The time response profile of individual particles (a short risetime followed by an exponential decay with decay parameter of about $\tau = 60$ ns) cannot be used to separate

the muonic and electromagnetic (EM) signal components since this profile is the same for all particles. There are two population features that can, on average, enable us to separate the two components: the amplitude distribution of the particle responses and the time-of-arrival distributions. The amplitude distribution of muons depends on the zenith angle, but in general it is close to a Gaussian of mean 1 VEM with a lower tail due to short-tracklength corner-clipping muons and a higher tail due to delta rays generated by high-energy muons. The mean amplitude of a single EM particle is much smaller (but with a power-like heavy tail), and the number of EM particles are, on average, an order of magnitude larger than the number of muons. With respect to the time-of-arrival distribution, typically, muons arrive earlier than EM particles. These two features make the muon signal peaky and short and the EM signal smooth and elongated. Both methods presented in Sections 2.1 and 2.2 use these features of the data to measure the muon fraction. There are several limitations of both methods that generate both variance and systematic bias between models and primaries (muon pile-up, small muon peaks due to corner-clipping muons, signal fluctuation), but the main source of uncertainty is due to high-energy photons that can produce a signal similar to that of a muon. Their contribution is estimated to be less than 10% to 15% for proton and iron primaries, respectively, in the considered energy and angular range.

2.1 Measuring the muon fraction with a multivariate method

The basic idea of this method is to combine muon-content-sensitive characteristics of the FADC signal to measure the muon fraction. Concretely, we estimate the muon fraction f_μ by

$$\hat{f}_\mu = a + b\,\hat{\theta} + c\,f_{0.5}^2 + d\,\hat{\theta}\,P_0 + e\,\hat{r}, \qquad (2)$$

where $\hat{\theta}$ is the reconstructed zenith angle of the shower and $\hat{r}$ is the distance of the detector from the reconstructed shower axis. $f_{0.5}$ is the portion of the signal in FADC bins larger than 0.5 VEM, that is,

$$f_{0.5} = \frac{1}{S}\sum_{j=1}^{N} x_j \mathbb{I}\{x_j > 0.5\}, \qquad (3)$$

where the indicator function $\mathbb{I}\{A\}$ is 1 if A is true and 0 otherwise. P_0 is the normalized zero-frequency component of the power spectrum, that is,

$$P_0 = \frac{S^2}{N\sum_{j=1}^{N} x_j^2} = \frac{\langle \mathbf{x}\rangle^2}{\langle \mathbf{x}^2\rangle} = \left[1 + \frac{\sigma^2(\mathbf{x})}{\langle \mathbf{x}\rangle^2}\right]^{-1}, \qquad (4)$$

where $\langle \mathbf{x}\rangle = S/N$ is the mean of the signal vector $\mathbf{x} = (x_1,\ldots,x_N)$, $\sigma^2(\mathbf{x})$ is the variance of the signal vector, and $\langle \mathbf{x}^2\rangle$ is its second moment. Both $f_{0.5}$ and P_0 are sensitive to large relative fluctuation and short signals, which are the signatures of high muon content. Besides the two parametrized families of thresholded signal and binned normalized power spectrum, we also tried other muon-content-sensitive families of variables, namely the time quantiles of the signal $t_q = \min\{t : \sum_{j=1}^{t/25\,\mathrm{ns}} x_j/S \geqslant q\}$ and thresholded discrete derivatives ("jumps" [5]) $J_\delta = \sum_{j=1}^{N-1}(x_{j+1} - x_j)\mathbb{I}\{x_{j+1} - x_j > \delta\}/S$. The formula Eq. (2) was selected by an exhaustive search among all quadratic functions over members of these parametrized families with the objective of minimizing the variance and the sensitivity of the estimator $\hat{f}_\mu$ to models and composition.

We estimate the fit parameters (a,b,c,d,e) using simulations (described in Section 3) in two steps. First we regress the muon fraction f_μ against $a + b\,\hat{\theta} + c\,f_{0.5}^2 + d\,\hat{\theta}\,P_0$ using a dense ring of 12 artificial detectors, placed at 1000 m from the shower axis. Then we fix b, c, and d, and regress f_μ against the full estimator $\hat{f}_\mu$ with free a and e using the detectors triggered by the shower. The reason for this two-step procedure is that we have much more dense detectors in the simulations, allowing us to control the statistical error of the fit in the first step, but these detectors are all placed at 1000 m from the core, so we cannot use them to estimate the distance dependence of the muon fraction. The overall bias of $\hat{f}_\mu - f_\mu$ on the different models and primaries is about ± 0.02 and the average resolution is about 0.08.

2.2 Measuring the muon fraction with a smoothing method

The basic idea of this method is to run a low-pass filter a few times on the signal to gradually separate the low-frequency smooth EM component from the high-frequency component which is assigned to muons. Formally, we first smooth the signal $\mathbf{x}$ by a moving average

$$\hat{x}_j = \sum_{i=1}^{N} x_i\,p_{ij} \qquad j = 1,\ldots,N, \qquad (5)$$

where $p_{ij} = \mathbb{I}\{|i-j| \leqslant L\}/C_j$. L is a tuned window size that depends on the zenith angle θ, and C_j is the size of the set $\{i : |i-j| \leqslant L\}$. The choice of L is driven by the physics of the air-showers: the amount of signal per time bin in the time distribution of the EM component decreases as the zenith angle grows, while the opposite happens to the muonic component. In the smoothing filter, lower frequency cuts correspond to larger convolute ranges. As a consequence, a wider window allows us to easily follow the low frequencies composing the EM signal at large angles, while narrower windows are needed to extract it in vertical showers, where the EM component is more similar to the muonic signal. As a consequence, we let the window size L grow with the zenith angle θ. The exact function $L = 7.83 + 0.09\,\theta/^\circ$ was tuned using simulations.

We assign any positive difference to the muonic signal, that is,

$$S_\mu = \sum_{j=1}^{N} \mathbb{I}\{x_j > \hat{x}_j\}\,(x_j - \hat{x}_j). \qquad (6)$$

We repeat the procedure four times, re-smoothing each time the smooth signal $\hat{x}_j$ from Eq. (5), output by the previous iteration. The final muonic signal is the sum of the non-smooth positive differences from Eq. (6). The muon fraction is then estimated by

$$\hat{f}_\mu = S_\mu/S. \qquad (7)$$

The overall bias of $\hat{f}_\mu - f_\mu$ on the different models and primaries is about ± 0.05 and the average resolution is about 0.08.

3 Simulations and data selection

The methods described in Section 2 were applied to detectors that are part of SD events passing fiducial cuts. The

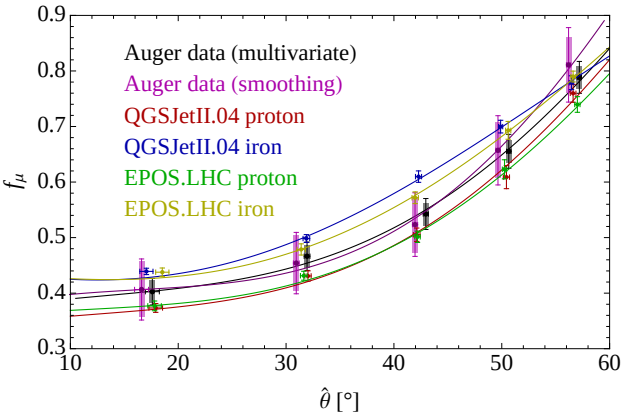

Figure 1: The muon fraction for primary energy $E = 10^{19}$ eV in a SD station at 1000 m from the shower axis, as a function of the reconstructed zenith angle $\hat{\theta}$. For Auger data, the rectangles represent the systematic uncertainties, and the error bars represent the statistical uncertainties added to the systematic uncertainties. The points for Auger data are artificially shifted by $\pm 0.5°$ for visibility. See Sections 2.1 and 2.2 for a detailed description.

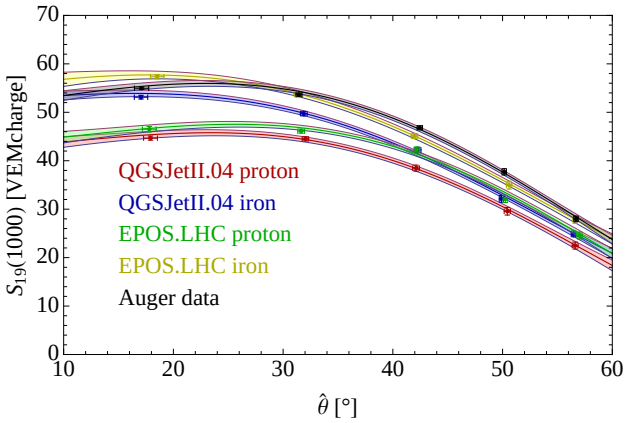

Figure 2: The mean total signal for primary energy $E = 10^{19}$ eV in a detector at 1000 m from the shower axis, as a function of the reconstructed zenith angle $\hat{\theta}$. See Section 4.2 for a detailed description.

cut requires that six active detectors surround the detector with the highest signal [9], which ensures a reliable core and energy reconstruction. The zenith angle, the energy, and the core position of the shower were reconstructed following the standard Auger SD reconstruction [10, 11]. We first selected events from the time period between Jan 2004 and Dec 2012 with zenith angle $\hat{\theta} < 60°$ and reconstructed energy $\hat{E} \in [10^{18.98}, 10^{19.02}]$ eV, then we selected detectors with a distance from the reconstructed shower axis $\hat{r} \in [950, 1050]$ m, giving us 521 SD signals. At $\hat{E} = 10^{19}$ eV, the resolutions for the core position and the energy are about 50 m and 12%, respectively. The absolute energy scale has a systematic uncertainty of 14% [8].

To tune and test the methods described in Section 2, we used four shower libraries generated with CORSIKA [12]: proton and iron showers using the hadronic models QGSJETII.04 [3] and EPOS LHC [4] with FLUKA [13] as the low-energy interaction model. The detector response of the showers was simulated [14] using GEANT4 [15] simulations within the Offline software framework [16] of the Auger Observatory. We used the same energy, angle, and distance cuts as in the data.

4 Results

In the following we will first present the results for the muon fraction f_μ and compare the Auger data with simulation predictions. In a next step we will derive the overall detector signal and multiply it by the measured muon fraction to derive the muon signal.

4.1 Measuring the muon fraction

We estimate the muon fraction $\hat{f}_\mu$ from Eqs. (2) or (7) for every detector in the distance range $\hat{r} \in [950, 1050]$ m. The muon fraction is a very slowly varying function of the lateral distance and energy, which allows us to calculate the mean muon fraction at a given zenith angle by averaging over the selected detectors and showers in a given angular interval.

The results for the muon fraction (f_μ for simulations and $\hat{f}_\mu$ for Auger data) are shown in Fig. 1 for $E = 10^{19}$ eV and $\hat{r} = 1000$ m.[1] The muon fraction varies between 0.3 and 0.9 as a function of the zenith angle. Good agreement is found for the muon fractions derived with the two analysis methods. The model predictions for proton- and iron-induced showers bracket the measured muon fractions within the systematic uncertainties.

4.2 Measuring the total signal

To obtain the total signal $S(1000)$ at 1000 m from the shower axis, we apply

$$S(1000) = S \times \mathrm{LDF}(1000\,\mathrm{m})/\mathrm{LDF}(\hat{r}), \qquad (8)$$

where $\hat{r}$ is the distance from the reconstructed shower axis, and $\mathrm{LDF}(r) = r^\beta$ is the lateral distribution function of the total signal, where $\beta = -3.45$ is obtained by fitting a power law on detector signals of the simulation libraries described in Section 3. We then rescale the total signal to 10^{19} eV by further multiplying $S(1000)$ by $C(E) = (E/10^{19}\,\mathrm{eV})^{-0.966}$ to obtain the *projected* total signal

$$S_{19}(1000) = S(1000) \times C(E), \qquad (9)$$

where the exponent -0.966 comes from the slope of the energy dependence of $S(1000)$ [10]. To correct the migration effect due to the steep slope of $E^{-2.6}$ of the energy spectrum [17] and the 12% energy resolution [10], we multiply the reconstructed energy by a factor of 0.984 before applying Eq. (9).

Fig. 2 depicts the projected total signal $S_{19}(1000)$ (for data and simulations) as a function of the reconstructed zenith angle. Note that none of the transformations in Eqs. (8) and (9) bias the mean total signal but they do decrease its variance.

For showers with primary energy $E = 10^{19}$ eV, the total signal S in a detector at 1000 m varies between 20 and 60 VEM, depending primarily on the zenith angle but also on the simulation model and on the mass composition of the primary particle (Fig 2). The mean signal in data is significantly higher than that of QGSJETII.04 proton

1. In all figures, showers are binned by their reconstructed zenith angle into bins determined by the borders [0°, 26°, 37°, 47°, 53°, 60°]. The x-coordinate of every point is the mean zenith angle in the bin.

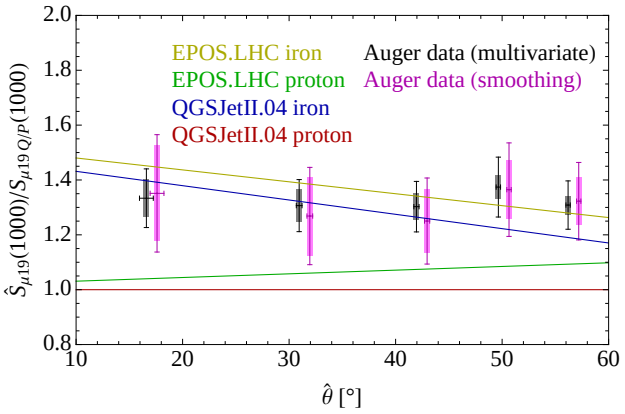

Figure 3: The measured muon signal rescaling at $E = 10^{19}$ eV and at 1000 m from the shower axis vs. zenith angle, with respect to QGSJETII.04 proton as baseline. The rectangles represent the systematic uncertainties, and the error bars represent the statistical uncertainties added to the systematic uncertainties. The points for Auger data are artificially shifted by $\pm 0.5°$ for visibility.

simulations and still exceeds somewhat that of iron-induced showers simulated with QGSJETII.04. The discrepancy is possible since the function that relates the ground signal to the primary energy is not determined by Monte Carlo, rather it is calibrated to the calorimetric energy measured by the fluorescence detector [17].

4.3 Computing the muon signal rescaling

In the QGSJETII.04 proton simulation, taken as a reference, we compute the muon fraction f_μ from Eq. (1) for every detector, and multiply it by the projected signal $S_{19}(1000)$ from Eq. (9) to obtain the projected muon signal

$$S_{\mu 19}(1000) = f_\mu \times S_{19}(1000). \qquad (10)$$

In the Auger data set, we compute the muon fraction estimate $\hat{f}_\mu$ from Eqs. (2) or (7) for every detector and multiply the fraction by the projected signal $S_{19}(1000)$ to obtain the estimated projected muon signal

$$\hat{S}_{\mu 19}(1000) = \hat{f}_\mu \times S_{19}(1000). \qquad (11)$$

Then we separate the detectors by the reconstructed zenith angles $\hat{\theta}$ of the corresponding showers into zenith angle bins, and divide the mean estimated muon signal $\langle \hat{S}_{\mu 19}(1000) \rangle$ in data by the mean muon signal $\langle S_{\mu 19}(1000) \rangle$ in the baseline simulation, properly accounting for the small effects of the unequal mean angles and the nonzero variance of the denominator.

The result of the analysis is shown in Fig. 3. The rectangles represent the systematic uncertainties, and the error bars represent the statistical uncertainties added to the systematic uncertainties. We determine that the measured factor of the muon signal in data divided by the muon signal in QGSJETII.04 proton showers at 10^{19} eV and at 1000 m in the full angular range of $[0°, 60°]$ is

1.33 $\pm$0.02 (stat.) $\pm$0.05 (sys.) (multivariate)
1.31 $\pm$0.02 (stat.) $\pm$0.09 (sys.) (smoothing)

5 Summary

The fraction of the muonic signal measured in the detectors of the Pierre Auger Observatory has been estimated from the time structure of the recorded signal for showers of 10^{19} eV in different zenith angle bins between 0° and 60°. Two methods, a multivariate technique and a smoothing technique, have been used to derive the fraction of the signal due to muons. The results of the two methods are in very good agreement. The measured fraction of the muonic to total signal is bracketed by model predictions for proton and iron primaries obtained with CORSIKA and QGSJETII.04 and EPOS LHC.

Combining the estimated muon signal fraction with the measured total signal at 1000 m from the shower core allowed us to derive the part of the detector signal that can be attributed to the muonic shower component. While the measured angular dependence of the muonic signal is found to be similar to the prediction obtained for proton showers and QGSJETII.04, the magnitude of the muonic signal is comparable to the predictions for iron showers.

Given that the observed distribution of the depth of shower maximum at 10^{19} eV is not compatible with an iron dominated composition [18] we conclude that the overall detector signal and the muonic signal are not well reproduced by the shower simulations. These results are compatible with that of the independent study for inclined showers whose signal at ground is dominated by muons [19, 20]. Comparing simultaneously the measured longitudinal shower profile and the surface detector signal to simulations provides further constraints on hadronic interaction models [6, 21].

Acknowledgment: B. Kégl was supported by the ANR-2010-COSI-002 grant of the French National Research Agency.

References

[1] R. Engel, D. Heck, and T. Pierog, Ann. Rev. Nucl. Part. Sci. **61** (2011) 467.
[2] The Pierre Auger Collaboration, Nucl. Instrum. Meth. A **523** (2004) 50.
[3] S. Ostapchenko, Nucl. Phys. Proc. Suppl. **151** (2006) 143.
[4] K. Werner, F. Liu, and T. Pierog, Phys. Rev. C **74** (2006) 044902.
[5] A. Castellina, for the Pierre Auger Collaboration, Proc. 31th ICRC, Łódź, Poland, 2009, arXiv:0906.2319.
[6] J. Allen, for the Pierre Auger Collaboration, Proc. 32th ICRC, Beijing, China, **2** (2011) 83, arXiv:1107.4804.
[7] X. Bertou *et al.* , Nucl. Instrum. Meth. A **568** (2006) 839.
[8] V. Verzi, for the Pierre Auger Collaboration, paper 0928, these proceedings.
[9] The Pierre Auger Collaboration, Nucl. Instrum. Meth. A **613** (2010) 29.
[10] R. Pesce, for the Pierre Auger Collaboration, Proc. 32th ICRC, Beijing, China, **2** (2011) 214, arXiv:1107.4809.
[11] M. Ave, for the Pierre Auger Collaboration, Proc. 30th ICRC, Mérida, Mexico, **1** (2007) 297, arXiv:0709.2125v1.
[12] D. Heck *et al.* , Wissenschaftliche Berichte, Forschungszentrum Karlsruhe FZKA 6019 (1998).
[13] A. Ferrari *et al.* CERN-2005-010.
[14] P. Billoir, Astropart. Phys. **30** (2008) 270.
[15] S. Agostinelli *et al.* , Nucl. Instrum. Meth. A **506** (2003) 250.
[16] S. Argirò *et al.* , Nucl. Instrum. Meth. A **580** (2007) 1485.
[17] The Pierre Auger Collaboration, Phys. Lett. B **685** (2010) 239.
[18] The Pierre Auger Collaboration, JCAP **1302** (2013) 026.
[19] G. Rodriquez, for the Pierre Auger Collaboration, Proc. 32th ICRC, Beijing, China, **2** (2011) 95, arXiv:1107.4809.
[20] I. Valiño, for the Pierre Auger Collaboration, paper 0635, these proceedings.
[21] G. Farrar, for the Pierre Auger Collaboration, paper 1108, these proceedings.